Geometry, electronic structure and thermodynamic stability of intrinsic point defects in indium oxide



2009 J. Phys.: Condens. Matter 21 455801

(http://iopscience.iop.org/0953-8984/21/45/455801)

IOP Publishing Journal of Physics: Condensed Matter

J. Phys.: Condens. Matter **21** (2009) 455801 (11pp) doi:10.1088/0953-8984/21/45/455801

# Geometry, electronic structure and thermodynamic stability of intrinsic point defects in indium oxide

**Péter Ágoston[1], Paul Erhart[2], Andreas Klein[1] and Karsten Albe[1]**

[1] Institut für Materialwissenschaft, Technische Universität Darmstadt, Petersenstraße 23, D-64287 Darmstadt, Germany

[2] Lawrence Livermore National Laboratory, L-367, Livermore, CA 94550, USA

Received 10 August 2009, in final form 28 September 2009

Published 23 October 2009

Online at stacks.iop.org/JPhysCM/21/455801

**Abstract**

Intrinsic point defects in indium oxide, including vacancies, interstitials as well as antisites, are studied by means of first-principles calculations within density functional theory using the generalized gradient approximation together with on-site corrections. Finite-size effects are corrected by an extrapolation procedure in order to obtain defect formation energies at infinite dilution. The results show that all intrinsic donor defects have shallow states and are capable of producing free electrons in the conduction band. This applies in particular to the oxygen vacancy. Since it has also a low formation energy, we find that the oxygen vacancy should be the major donor in this material explaining the n-type conductivity as well as the non-stoichiometry of indium oxide. In addition, we show that there are a wealth of oxygen dumbbell-like defects which are thermodynamically relevant under oxidizing conditions. Finally, we discuss defect induced changes of the electronic structure.

(Some figures in this article are in colour only in the electronic version)

## 1. Introduction

Indium oxide ($In_2O_3$) is a transparent conducting oxide (TCO), similar to tin oxide and zinc oxide. TCOs exhibit high electrical conductivities while lacking optical excitations within the visual range [1, 2]. In optoelectronics, and especially for applications involving organic materials such as organic light emitting diodes (OLEDs) [3] and organic photovoltaics (OPVs) [4, 5], Sn-doped indium oxide (ITO) is the primary choice [6]. For this material free electron-like conductivities have been measured [7] with carrier concentrations on the order of $10^{21}$ cm$^{-3}$. In addition, $In_2O_3$ is a suitable material for gas sensing applications especially of oxygen and ozone [8].

It is a remarkable feature of $In_2O_3$ that even the undoped material is n-type conducting [9] with carrier concentrations of up to $10^{19}$ cm$^{-3}$. The preference for n-type conduction has been attributed to intrinsic donor defects, which have also been invoked to explain the pronounced non-stoichiometry observed under highly reducing conditions [10].

From the experimental point of view, both the non-stoichiometry and the n-type conductivity have been assigned to doubly charged oxygen vacancies [9]. Oxygen related defects are also conjectured to be of importance for gas sensing applications [8], and may play a crucial role in the fatigue of devices with functional organic materials [11].

Because of these experimental findings, the oxygen vacancy in $In_2O_3$ received particular attention in early theoretical studies [12, 13]. Further investigations considered defect complexes of oxygen vacancies and indium interstitials [14]. None of these studies, however, addressed the thermodynamic stability of point defects as well as their electronic transitions. Only recently, these issues were addressed in a study by Lany and Zunger [15]. Based on first-principles calculations within density functional theory (DFT) they concluded that no intrinsic point defect is capable of producing the high electron densities experimentally observed in reduced samples. In addition, they suggested that conductivity should originate from a photo-induced process: according to their calculations, the oxygen vacancy acts as neutral color center binding two electrons. Then, upon successive absorption of two photons a persistent conductivity should be obtained, since a large energy barrier is associated with the relaxation process. To the best of our knowledge, no direct evidence for such a mechanism

 

in $In_2O_3$ has been found so far. Moreover, this explanation is based on a value of 3.5 eV for the experimental band gap. A recent study, however, have revealed the existence of forbidden optical transitions [16] and a fundamental band gap of 2.8–2.9 eV, which is consistent with optical reflectivity of $In_2O_3$ single crystals and XPS studies [17, 18], as well calculated quasiparticle band structures of a rhombohedral polymorph [19].

In contrast to other TCOs, like ZnO, the defect chemistry of $In_2O_3$ has not been studied in full detail and many open questions remain. Therefore the primary goal of the present work is to carry out an extensive study on intrinsic point defects in $In_2O_3$ with particular focus on their thermodynamic and structural properties. To this end we have conducted calculations on the basis of density functional theory (DFT) using the GGA + $U$ method to achieve a better description of the electronic structure of the material. We consider not only vacancies and interstitials on high-symmetry positions, but also antisites, defect associates of donor defects over a wide range of conceivable charge states. Since our previous studies on ZnO have revealed that covalently bonded oxygen interstitial geometries are potentially important intrinsic defects [20], a variety of low-symmetry configurations of oxygen interstitial defects were included in our calculations. Based on these data we develop a complete and consistent picture of the intrinsic defect chemistry of $In_2O_3$.

## 2. Methodology

### 2.1. Computational setup

Density functional theory (DFT) calculations were carried out using the Vienna *ab initio* simulation package (VASP) [21, 22]. The potentials due to the nuclei and the core electrons were represented by the projector augmented wave (PAW) scheme by Blöchl [23, 24]. The 4d, 5s, and 5p electrons of indium as well as the 2s and 2p electrons of oxygen were treated as part of the valence, while the plane wave cut-off energy was set to 500 eV. The generalized gradient approximation (GGA) in the parametrization by Perdew, Burke and Ernzerhof (PBE) [25] was selected to express the exchange–correlation potential. Since the 'standard' GGA functional underestimates the binding energy of In 4d electrons, which leads to a considerable overestimation of the O 2p–In 4d hybridization, we adopted the GGA + $U$ method in the formulation by Dudarev *et al* [26] with $\bar{U} - \bar{J} = 7$ eV. This approach has been successfully used in a recent study of the valence band structure of $In_2O_3$ [27]. In order to evaluate the effect of this on-site correction, we additionally performed standard GGA calculations for comparison. For Brillouin-zone integrations, a Γ-centered 3 × 3 × 3 $k$-point mesh was employed, which proved to be sufficient also for defect calculations. Especially, the defect formation energies change negligibly when larger or shifted meshes are used. The properties of bulk $In_2O_3$, which have been calculated using these computational parameters, are summarized in table 1 and compare very well with experimental data.

**Table 1.** Comparison of calculated and experimentally measured properties of indium oxide, indium and oxygen. Calculations for the compound and the elements were carried out using the generalized gradient correction (GGA). Additional calculations for the compound were performed using the GGA + $U$ method. $E_c$: cohesive energy (eV/f.u.), $\Delta H^f$: compound formation energy (eV/f.u.), $E_G$: band gap (eV), $a_0$: lattice constant (Å), $c/a$: axial ratio, $V_0$: unit cell volume (Å$^3$), $D_0$: dimer dissociation energy (eV), $r_0$: dimer bond length (Å).

| | Experiment | GGA | GGA + $U$ |
|---|---|---|---|
| Indium oxide (bixbyite, $Ia\bar{3}$) | | | |
| $E_c$ | | −28.27 | −29.29 |
| $a_0$ | 10.121[a] | 10.306 | 10.027 |
| $V_0$ | 64.80[a] | 68.41 | 63.01 |
| $E_G$ | 2.5–3.75[b] | 0.93 | 1.79 |
| $\Delta H^f$ | −9.596[c] | −9.61 | −10.63 |
| Indium (tetragonal, $I4/mmm$) | | | |
| $E_c$ | | −2.728 | |
| $a_0$ | 3.332[c] | 3.281 | |
| $c/a$ | 1.342[c] | 1.479 | |
| $V_0$ | 49.644[c] | 52.238 | |
| Oxygen (dimer) | | | |
| $D_0$ | 5.17[c] | 4.4 | |
| $r_0$ | 1.208[c] | 1.23 | |

[a] Reference [50]. [b] Reference [17].
[c] Reference [51].

### 2.2. The GGA + U method

Since spurious self-interactions are partly responsible for the discrepancies between calculated and experimental band structure, the GGA + $U$ method [28, 29] was used within the present work to remedy some of this error. Within Dudarev's approach [26], there is only one free orbital dependent parameter, $\bar{U} - \bar{J}$, which can be varied. $\bar{U}$ and $\bar{J}$ are the spherically averaged matrix elements of the screened Coulomb electron–electron interaction. The band structure of indium oxide is described well within the GGA except for two aspects. Firstly, the indium 4d semi-core bands are too close to the VBM as compared to experimental photoelectron spectroscopy data. Further, the calculated band gap turns out to be only one third of the experimental value (0.93 eV instead of 2.8 eV). Although this underestimation of excited states is well known for DFT, the error is exceptionally high. In $In_2O_3$, the indium 4d semi-core band, which is strongly affected by unphysical self-interaction is pushed to lower energies when the difference $\bar{U} - \bar{J}$ is increased. In d states also contribute to the upper valence band structure and therefore influence the bonding in the material. Since structural relaxation and rebonding during defect formation is important, all defect calculations were performed using the semi-empirical on-site correction for In 4d orbitals. As we have showed [27], for $\bar{U} - \bar{J} = 7$, the electronic density of states agrees very well with experimental data of [30, 31]. Furthermore, the band gap is also widened and the lattice constant is reduced giving a better overall description of the structure as compared to GGA-only calculations.

*2.2.1. Defect calculations.* The defect calculations were carried out with fixed cell parameters as obtained for the ideal structure while the ionic positions were optimized until the maximum force was converged to less than 10 meV $Å^{-1}$. Under ambient conditions $In_2O_3$ assumes the bixbyite structure ($Ia\bar{3}$, space group no. 206). The primitive unit cell contains 40 atoms whereas the conventional (bcc) unit cell contains 80 atoms. Calculations were carried out using four different cell sizes in order to assess the effect of finite system size. The first two cells are based on the 80-atom conventional cubic unit cell ($1 \times 1 \times 1$ and $1 \times 1 \times 2$), while the other two cells are multiples of the primitive 40-atom unit cell ($1 \times 1 \times 1$ and $3 \times 1 \times 1$). For calculating charged defects, a homogeneous background charge was added to ensure overall charge neutrality. In order to remedy the effect of unphysical elastic and/or electrostatic interactions between periodic images, an extrapolation scheme [32] was applied to obtain the defect formation energies at infinite dilution: to this end, we first added the monopole–monopole correction term [33, 34], and in case of charged defects corrected the valence band maximum ($E_{VBM}$) by a band-alignment procedure [35]. Then the formation energies were subjected to finite-size scaling with respect to the inverse system volume to account for monopole–quadrupole and electrostatic interactions. The monopole–monopole interaction is screened by the static dielectric constant, for which we used the experimental value of $\epsilon = 8.9$ determined by optical measurements [1]. An extensive discussion and further details pertaining to the extrapolation procedure can be found in [32].

*2.2.2. Analysis of charge transfer and transition barriers.* In order to analyze the charge redistribution and localization upon defect formation, Bader charges were calculated [36]. With this method a formal oxidation number can be introduced by evaluating the charge within the Bader volume of the ions for the ideal cell. For bulk indium oxide 7.2 and 11.1 electrons were obtained for oxygen and indium ions, respectively. This value can be compared with the number of valence electrons per atom (6 for O and 13 for In) in the calculation. The significant amount of charge transfer indicates the ionicity of the system.

As will be shown below, there are various oxygen interstitial configurations with very similar formation energies. In order to calculate the transition barriers between these structures, we used the climbing image nudge elastic band method (CI-NEB) with up to five images [37–39].

### 2.3. Formation energies

The Gibbs free energy for the creation of a point defect with charge $q$ in the two component system $In_2O_3$ is given by [40, 41]

$$\Delta G_D = G_{def} - G_{host} - \Delta n_{In}\mu_{In} - \Delta n_O\mu_O + q(E_{VBM} + E_F), \quad (1)$$

where $G_{host}$ and $G_{def}$ are the total free energies of the ideal and the defective supercells, respectively, $\mu_i$ are the chemical potentials, and $\Delta n_i$ denotes the change of the number of atoms of type $i$ from the ideal to the defective system. It is convenient to express the chemical potentials with respect to the ground states of the components, i.e. $\mu_i = \mu_i^0 + \Delta\mu_i$, where $\mu_O^0$ is given by the energy per atom of the oxygen dimer molecule, and $\mu_{In}^0$ is determined by the cohesive energy of metallic indium (see table 1). For charged defects ($q \neq 0$), the formation energies depend linearly on the chemical potential of the electrons $E_F$, which is measured with respect to the valence band maximum $E_{VBM}$.

The chemical potentials are subject to the thermodynamic boundary condition that the chemical potential of the compound $\mu_{In_2O_3}^0$ equals the chemical potentials of the constituents, i.e. $\mu_{In_2O_3}^0 = 2\mu_{In} + 3\mu_O$. Using the definition of the formation energy of the compound, $\Delta G^f = \mu_{In_2O_3}^0 - 2\mu_{In}^0 - 3\mu_O^0$, this yields

$$\Delta G^f = 2\Delta\mu_{In} + 3\Delta\mu_O. \quad (2)$$

The chemical potentials of In and O are therefore dependent on each other. Two limiting cases can be considered: in the oxygen rich limit $\mu_O = \mu_O^0$ and it follows that $\Delta\mu_O = 0$ and $\Delta\mu_{In} = \Delta G^f/2$, whereas in the indium rich limit the opposite holds, $\Delta\mu_O = \Delta G^f/3$ and $\Delta\mu_{In} = 0$.

The free energy of formation comprises the formation energy $\Delta E_D$, the formation entropy $\Delta S_D$, and the formation volume $\Delta V_D$ according to

$$\Delta G_D = \Delta E_D - T\Delta S_D + p\Delta V_D, \quad (3)$$

where $T$ and $p$ denote temperature and pressure, respectively. Since the formation energy $\Delta E_D$ is by the far the most important term, in the following we focus on this part only, that is we approximate $\Delta G_D \approx \Delta E_D(T = 0\,K)$.

## 3. Results and discussion

### 3.1. Thermodynamic stability

The Fermi level dependence of the formation energies calculated using equation (1) is shown in figure 2 for both oxygen and indium rich conditions. The data includes the monopole–monopole correction term and was subjected to a band-alignment procedure and finite-size scaling as described in section 2.2 (also compare table 2). For comparison, also GGA results are shown in the top part of the figure. In the indium rich regime (reducing conditions) oxygen vacancies display the lowest formation energy. Their formation energy is negative throughout the calculated band gap using GGA, and negative in major parts using GGA + $U$, pinning the Fermi level above the gap center. Competing donor defects like indium interstitials and indium antisites do always have higher formation energies than the oxygen vacancy. High formation energies are found for acceptor defects. Among them the oxygen interstitial on $c$-sites (figure 1) displays the lowest formation energy. Both, the indium vacancy and the oxygen interstitial acceptor defects cross the zero-energy line for Fermi levels located within the conduction band denoting the natural n-type doping limit. Under oxygen rich conditions (oxidizing conditions), neutral oxygen interstitials

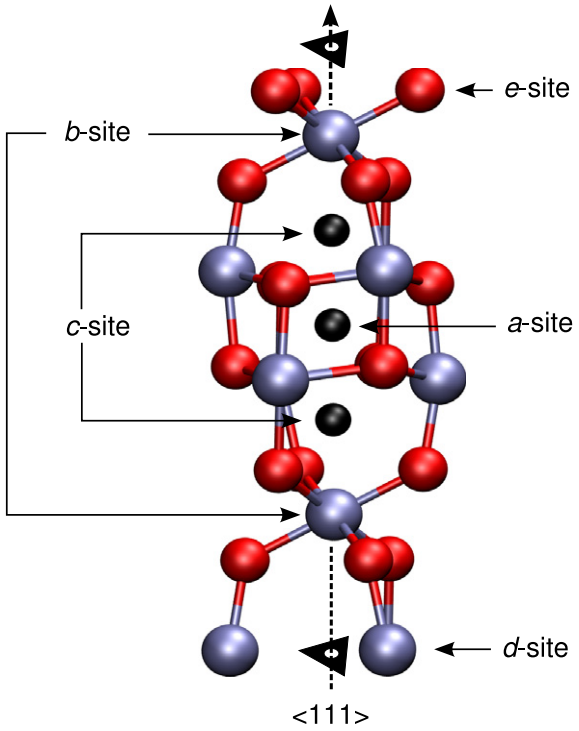


**Figure 1.** Arrangement of atoms surrounding the ⟨111⟩ threefold axis. Black spheres denote interstitial sites enclosed by two regular indium *b*-sites in the order *b*–*c*–*a*–*c*–*b*. Indium atoms are also located on *d*-sites which have a two-fold point symmetry. Oxygen atoms reside on the low-symmetry *e*-site.

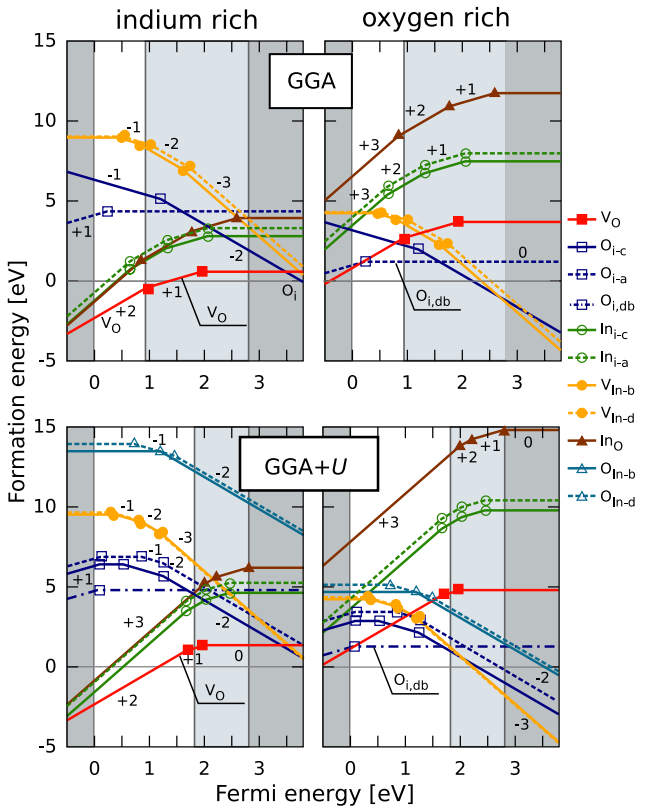


**Figure 2.** Fermi level dependence of formation energies under indium and oxygen rich conditions calculated with GGA + $U$ and GGA only. The data shown include monopole–monopole and finite-size scaling corrections. The most predominant defects are marked within the diagram, which is the oxygen vacancy in the indium rich limit and the oxygen dumbbell interstitial in the oxygen rich limit. The white strip indicates the calculated band gaps, which is 0.93 eV (GGA) and 1.81 eV (GGA + $U$). The difference to the experimental band gap is indicated by light gray shading. Dark areas represent the valence and conduction bands. The VBM is located at $E_F = 0$.

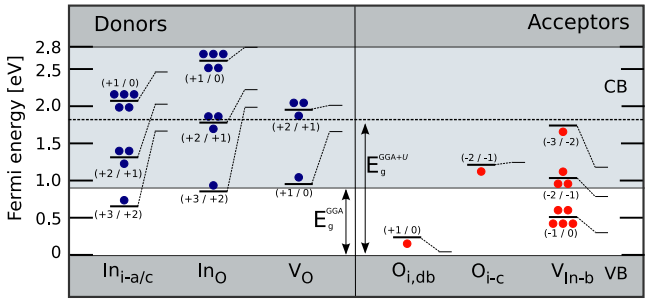


**Figure 3.** Transition energies for the major defects and their shifts upon application of the GGA + $U$ on-site correction. The circles below and above the transition levels denote the occupancy of the corresponding defect level for Fermi energies below and above, respectively. On the donor side, electrons occupy the defect state, whereas holes are depicted on the acceptor side. Transition energies for donors consistently shift upwards tracking the conduction band, where acceptor states shift downwards. The shifts of acceptor levels are generally smaller compared with donor levels.

in a dumbbell conformation are the dominant defect. Further, the maximum Fermi level position is calculated at ∼2.2 eV, which is good agreement with the lowest values observed by photoemission [42].

Qualitatively, GGA + $U$ does not change the overall picture. Especially acceptor defects retain mainly the same formation energies, whereas donor defects show higher formation energies for lower charge states, if calculations are performed using GGA + $U$.

The Fermi level position is determined by the overall charge neutrality condition, and therefore by the charged defects with the lowest formation energies. The electronic properties of the major defects can be seen in figure 3, where the Fermi level positions are shown at which charging or decharging of the defects occurs. Furthermore, circles indicate the occupancy of the corresponding defect levels for Fermi levels below and above the transition state respectively. All donor defects are shallow in the sense that they are positively charged for Fermi levels within the band gap and can therefore inject electrons into the conduction band. Comparing the results of GGA with GGA + $U$ calculations, it can be seen that all donor levels undergo upward shifts which conserve their electronic properties. It is especially noteworthy, that the stability region of the $q = +1$ charge state for the oxygen vacancy is strongly reduced using GGA + $U$. Finally, the oxygen dumbbells form a special class of defects, since they are not charged and do not contribute to the charge neutrality condition. Their equilibrium concentration is independent of Fermi level position for a given oxygen chemical potential.

### 3.2. Geometry and electronic structure

*3.2.1. Donor defects.* Indium oxide is a very good n-type conductor even in the absence of extrinsic dopants. Intrinsic

**Table 2.** Cell size corrected and uncorrected formation energies calculated with GGA + $U$. Values in parentheses give the corresponding GGA values. The uncorrected values were obtained using the 40 atom primitive unit cell. All values are given in eV for the indium rich ($H_f^{In}$) and oxygen rich ($H_f^{O}$) limiting cases.

| | | Corrected | | | | Uncorrected | | | |
|---|---|---|---|---|---|---|---|---|---|
| Defect | Charge | $H_f^{In}$ (eV) | | $H_f^{O}$ (eV) | | $H_f^{In}$ (eV) | | $H_f^{O}$ (eV) | |
| $V_O$ | 0 | 1.34 | (0.58) | 4.81 | (3.72) | 1.44 | (0.92) | 4.91 | (4.05) |
| | +1 | −0.66 | (−1.35) | 2.80 | (1.77) | −0.45 | (−1.08) | 3.01 | (2.04) |
| | +2 | −2.32 | (−2.30) | 1.14 | (0.82) | −1.76 | (−2.14) | 1.71 | (0.99) |
| $O_{i,db}$ | 0 | 4.76 | (4.36) | 1.28 | (1.23) | 4.80 | (4.49) | 1.33 | (1.35) |
| | +1 | 4.70 | (4.13) | 1.23 | (1.01) | 4.69 | (4.36) | 1.21 | (1.23) |
| $O_{i-c}$ | −2 | 8.12 | (7.54) | 4.64 | (4.41) | 8.82 | (8.13) | 5.34 | (4.99) |
| | −1 | 6.87 | (6.33) | 3.40 | (3.20) | 7.07 | (6.39) | 3.60 | (3.26) |
| | 0 | 6.35 | | 2.88 | | 6.21 | | 2.74 | |
| | +1 | 6.26 | | 2.79 | | 6.19 | | 2.72 | |
| | +2 | 6.75 | | 3.27 | | 6.96 | | 3.49 | |
| $O_{i-a}$ | −2 | 8.92 | | 5.44 | | 10.04 | | 6.56 | |
| | −1 | 7.67 | | 4.20 | | 8.11 | | 4.64 | |
| | 0 | 6.81 | | 3.34 | | 7.08 | | 3.61 | |
| $In_O$ | 0 | 6.14 | (3.94) | 14.82 | (11.77) | 6.96 | (5.07) | 15.65 | (12.91) |
| | +1 | 3.35 | (1.34) | 12.03 | (9.17) | 3.70 | (2.35) | 12.38 | (10.18) |
| | +2 | 1.13 | (−0.42) | 9.81 | (7.40) | 0.90 | (0.25) | 9.58 | (8.09) |
| | +3 | −0.85 | (−1.27) | 7.82 | (6.55) | −1.02 | (−0.94) | 7.65 | (6.88) |
| | +4 | 0.45 | | 9.13 | | −0.35 | | 8.33 | |
| | +5 | 0.34 | | 9.02 | | 0.69 | | 9.37 | |
| $V_{In-b}$ | −3 | 11.85 | (12.30) | 6.64 | (7.60) | 10.60 | (12.04) | 5.40 | (7.34) |
| | −2 | 10.67 | (10.56) | 5.46 | (5.87) | 9.52 | (10.35) | 4.31 | (5.65) |
| | −1 | 9.88 | (9.54) | 4.67 | (4.84) | 9.15 | (9.32) | 3.94 | (4.62) |
| | 0 | 9.57 | (9.03) | 4.36 | (4.33) | 9.48 | (8.91) | 4.27 | (4.21) |
| $V_{In\ d}$ | −3 | 11.92 | (11.79) | 6.71 | (7.09) | 10.79 | (11.81) | 5.58 | (7.11) |
| | −2 | 10.70 | (10.20) | 5.49 | (5.50) | 9.53 | (10.32) | 4.33 | (5.62) |
| | −1 | 9.82 | (9.40) | 4.61 | (4.70) | 9.08 | (9.28) | 3.87 | (4.58) |
| | 0 | 9.44 | (8.97) | 4.23 | (4.27) | 9.37 | (8.87) | 4.17 | (4.17) |
| $In_{i-c}$ | 0 | 4.58 | (2.81) | 9.79 | (7.51) | 6.31 | (4.60) | 11.52 | (9.30) |
| | +1 | 2.13 | (0.74) | 7.34 | (5.44) | 2.36 | (1.50) | 7.57 | (6.20) |
| | +2 | 0.10 | (−0.55) | 5.31 | (4.14) | −0.52 | (−0.45) | 4.68 | (4.24) |
| | +3 | −1.56 | (−1.20) | 3.64 | (3.49) | −2.08 | (−1.06) | 3.12 | (3.63) |
| $In_{i-a}$ | +2 | 0.50 | | 5.70 | | 0.16 | | 5.37 | |
| | +3 | −0.92 | | 4.28 | | −1.45 | | 3.75 | |
| $O_{In-b}$ | −2 | 16.01 | | 7.33 | | 16.01 | | 7.33 | |
| | −1 | 14.55 | | 5.86 | | 14.55 | | 5.86 | |
| | 0 | 13.82 | | 5.14 | | 13.82 | | 5.14 | |
| $O_{In\ d}$ | −2 | 15.77 | | 7.09 | | 15.77 | | 7.09 | |
| | −1 | 14.35 | | 5.86 | | 14.21 | | 7.33 | |
| | 0 | 13.38 | | 4.70 | | 13.38 | | 4.70 | |
| $O_{i,db1}$ | −1 | 8.40 | | 4.93 | | | | | |
| | 0 | 5.07 | | 1.60 | | | | | |
| | +1 | 4.88 | | 1.41 | | | | | |
| $O_{i,db2}$ | −1 | 9.02 | | 5.54 | | | | | |
| | 0 | 5.68 | | 2.21 | | | | | |
| | +1 | 4.88 | | 1.41 | | | | | |
| $In_{i-b,split}$ | 0 | 5.44 | | 10.65 | | | | | |
| | +1 | 2.26 | | 7.47 | | | | | |
| | +2 | −0.05 | | 5.15 | | | | | |
| | +3 | −1.43 | | 3.77 | | | | | |
| $In_{i-d}$ | +2 | 0.74 | | 5.95 | | | | | |
| | +3 | −0.85 | | 4.34 | | | | | |
| $[V_O]_2$ | 0 | 2.92 | | 9.86 | | 2.94 | | 9.88 | |
| | +1 | 0.28 | | 7.23 | | 0.84 | | 7.78 | |
| | +2 | −1.72 | | 5.22 | | −0.78 | | 6.16 | |
| | +3 | −1.94 | | 5.00 | | −0.56 | | 6.38 | |
| | +4 | −2.20 | | 4.74 | | −0.01 | | 6.92 | |

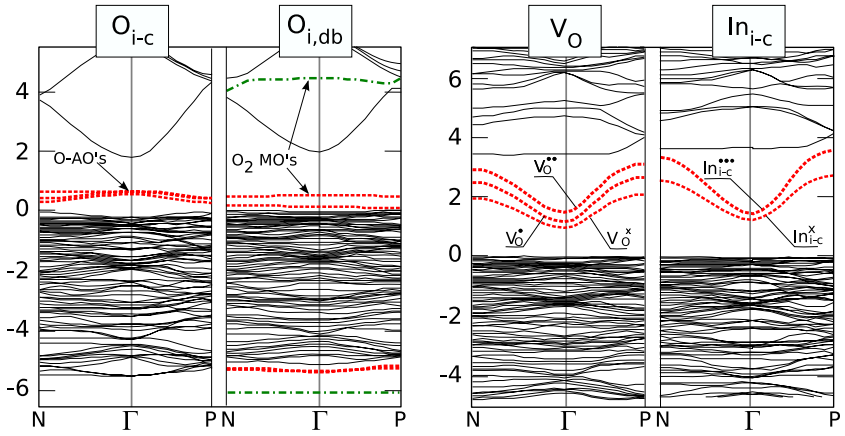


**Figure 4.** Electronic band structures of oxygen interstitials on symmetric site and in dumbbell configuration (left). Both defects produce valence band related gap states. For the dumbbell interstitial the states are extremely localized and resemble the molecular orbitals of doubly negative charged peroxo-ions ($O_2^{2-}$). On the right, band structures are shown with oxygen vacancy and indium interstitial including level relaxation at different charge states. Both defects open a second gap at higher energies and show a similar level relaxation upon occupation with electrons.

donor defects, therefore, deserve particular attention. The oxygen vacancy is a shallow donor, since it has a low formation energy and exhibits transitions to lower charge states directly at the calculated CBM. Indium interstitials, in comparison, have significantly higher formation energies.

Within the bixbyite lattice there are four distinct interstitial sites: the *c*-position is usually referred to as the structural vacancy site, which is occupied in the corresponding fluorite lattice. The *a*-site denotes the position of an inversion center as shown in figure 1 and is a potential interstitial site. Finally, interstitials can be placed on the two-fold axis along ⟨100⟩ on the connection line between two *d*-site indium lattice sites as well as along ⟨111⟩ directions as split interstitial on a *b*-site. The latter two defects are presented in figure 5.

The *c*-site position is most favorable for In interstitials followed by *b*-site split interstitial (+0.2 eV), *a*-site (+0.49 eV) and *d*-site (+0.75 eV). Generally, indium interstitials cause a significant lattice strain. In the case of the neutral *c*-site interstitial, the first neighbor shell, which consists of oxygen atoms, relaxes outward by about 10% (of original bond length). In the second shell the In atoms on *d*-sites display a 13% outward relaxation while the In atoms on *b*-sites move even 26% outward. Further, ions at yet larger distances are significantly affected.

For increasing charge states there is significant charge dependent relaxation which is of opposite sign for oxygen and indium neighbors. Anions are pulled inward (up to 16%) while cations are pushed outwards (2.5%).

In contrast, the geometry hardly changes for a neutral oxygen vacancy (−2.5% and −1.7% of original distance for cations and anions, respectively). The relaxation is not fully isotropic and results in a slight displacement of the geometric center of the vacancy. For higher charge states anions are again pulled inwards (up to 8%) while cations are pushed outwards (up to 10%). The relaxation also affects farther neighbor shells and occurs gradually with changing charge state. There is no evidence for rebonding in any charge state and charge dependent relaxation can mainly be seen as the result of ionic screening. The present calculations do therefore not reproduce the observations reported by Lany *et al* [15, 43].

If one compares the electronic structure of oxygen vacancies and indium interstitials (figure 4) the similarity of the two donor defects is apparent. Both defects induce a notable change in the band structure as compared with the ideal structure. Apart from the fundamental band gap, which is decreased due to the introduction of the defects, a second gap emerges inside the conduction band. A similar effect has been observed for Sn dopants [44]. This additional gap is produced by the hybridization of In 5s states with defect states [44]. The gap is larger for the oxygen vacancy (1.47 eV for the oxygen vacancy compared with 1.03 eV for the indium interstitial in neutral charge states). Figure 4 also shows the similar charge dependent level relaxation for the two donors. It is also instructive to compare the band structures found from the defect calculations with the band structure of Sn-doped $In_2O_3$ [44] which merely reveals a slight variation of the width of the secondary gap. Despite of these variations we do not find any evidence that vacancies have a different electronic behavior than indium interstitials as proposed by Lany *et al* [15]. On the contrary, our findings show that both donors produce delocalized conduction band related defect states. This is consistent with the formation energies, as it was shown (see figure 2) that both defects are more stable if they are ionized and transition states mainly follow the conduction band edge upon GGA + *U* correction. As the band gap is underestimated by DFT and there is no consensus with regard to the actual band gap we will not include band gap corrections. Assuming rigid levels, one would however expect donor and acceptor levels to track the conduction and valence band edges, respectively.

*3.2.2. Defect associates.* Although $In_2O_3$ is highly ionic [30], antisite configurations exhibit remarkably low formation energies and the indium antisite can act as a donor defect inducing non-stoichiometry (see figures 2 and 5).

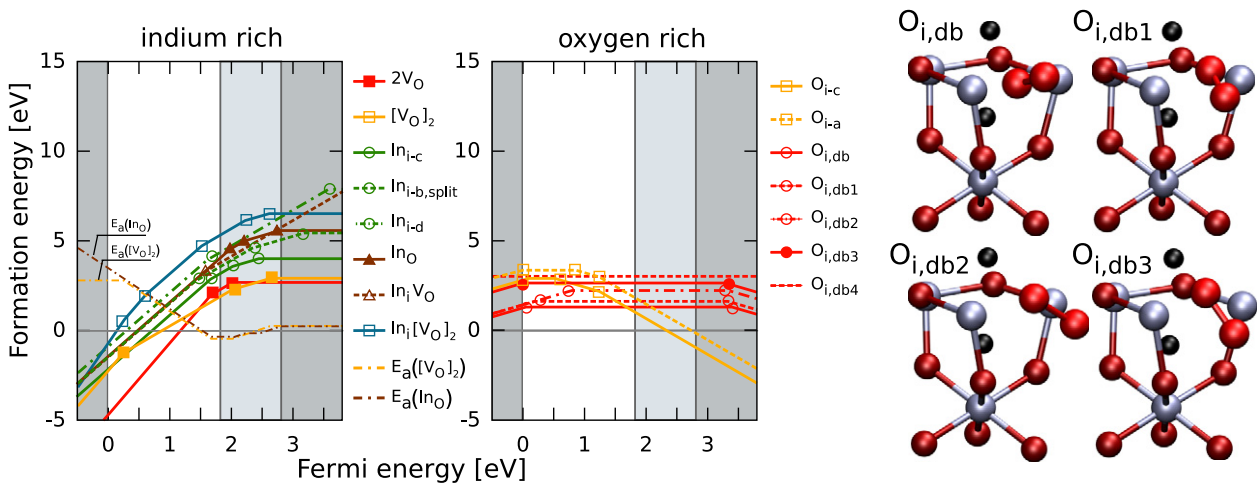


**Figure 5.** Dependence of formation energy with Fermi level for defects and defect complexes (left). Here, the formation energy of two separated oxygen vacancies is compared with the formation energy of a di-vacancy. For Fermi energies higher than 1.5 eV there is a small negative association energy ($E_a$), whereas there is increasing repulsion at lower Fermi energy. A similar behavior is found for the antisite ($In_O$). Indium *b*-site split interstitials and *d*-site interstitials have slightly higher formation energies compared with *c*-site interstitials. Formation energies of oxygen interstitial defects are shown in the oxygen rich limit (middle). Throughout the whole calculated band gap oxygen dumbbell defects are the major defect types. Four of these defects ($O_{i,db}$, $O_{i,db1}$, $O_{i,db2}$, $O_{i,db3}$) have lower formation energies than regular oxygen interstitials on *c*-/ *a*-sites, and differ mainly by the orientation of the dimer axis.

Stable antisites were also found in $SnO_2$ and can be explained by the multivalence of tin [45]. Since indium itself also possesses a lower oxidation number which manifests for example in the more oxygen deficient compound $In_2O$, a similar behavior can be expected. Energetically, the indium antisite ($In_O$) is very close to the interstitial with comparable transition energies. The relaxation behavior of the defect, however, is different. In the case of the antisite, the relaxation process is highly non-symmetric. The energy minimum for this defect configuration is strongly displaced from the regular oxygen site resulting in an indium interstitial oxygen vacancy defect pair. Surprisingly, the minimum energy is not at a regular interstitial *c*-position. The surplus indium atom moves within the {111} plane and aligns with the two-fold rotation axis along ⟨100⟩ (a configuration similar to the *b*-site interstitial). If one compares the formation energies of indium interstitials and oxygen vacancies with the oxygen antisites (figure 2), it is evident that there is no association energy ($E_a$) for neutral defect pairs, as the sum of the formation energies equals that of the antisite ($V_O$–$In_i$ defect complex). At the conduction band edge, however, there is an association energy of about 0.3 eV indicating some tendency for association.

The low formation energy of the indium antisite defect motivated further investigations of other defect associates. Surprisingly, the combination of an oxygen vacancy with an indium interstitial on a regular *c*/*a*-site does not result in lower formation energies when compared with the antisite.

Finally, the association of oxygen vacancies to di-vacancies was studied, since donor concentrations are expected to be high in $In_2O_3$. Several configurations with distinct nearest neighbor configurations can be constructed, which practically do not differ in their formation energies. The Fermi level dependence of the formation energy for one representative di-vacancy configuration ($[V_O]_2$) is included in figure 5. For comparison the formation energy is also shown for the infinitely separated oxygen vacancies (sum of two single defects). For low Fermi energies there is an increasing repulsion whereas a weak interaction (∼0.3 eV) is observed for high Fermi energies near the CBM. In real samples, a high concentration of oxygen vacancies is found together with a high Fermi energy, so that formation of di-vacancies is expected under these conditions.

Although indium interstitials and indium antisites have rather high formation energies, interstitials and antisites could also contribute to the n-type conductivity of the material, since the deposition of $In_2O_3$ films is a far-from-equilibrium process. Especially for the antisite a low mobility can be expected.

*3.2.3. Acceptor-like defects.* Acceptor defects are important, because their presence affects the dopability of the material by charge compensation. Furthermore, oxygen interstitials form the most abundant defect types under oxidizing conditions and can attain charge states other than $q = -2$.

For the case of oxygen interstitials on symmetric *c*/*a*-sites, the surplus oxygen encloses a net charge equivalent to the charge of a reference oxygen in an ideal cell. In other words, the interstitial has an oxidization state similar to an oxygen on a regular lattice site for the same total charge state of the cell. Hence the major part of the surplus electrons is well localized on the interstitial. For less negative charge states the electron density is significantly reduced not only at the interstitial but also at first and second neighbors. On the other hand, for neutral and positive interstitials, charge is withdrawn from neighboring atoms resulting in a configuration with delocalized charge and less ionic relaxation.

Consistently, the introduction of a neutral oxygen leads to some outward relaxation (8%). The relaxation mainly occurs within the second neighbor oxygen shell, while displacements

on nearest neighbor indium atoms are smaller than 1%. This configuration remains unchanged for more positive charge states. For negative charge states, due to strong charge localization, indium atoms move towards the interstitial site (8%) and oxygen neighbors are pushed farther outwards by 5%. Additionally, constrained by symmetry, the *c*-site interstitial moves along the [111] axis towards the *a*-site (figure 1) for increasingly negative charge states whereas it is located at the geometric center for the charge state $q = 2$.

There is an alternative way of accommodating electron deficiency for oxygen interstitial defects. In the oxygen rich regime oxygen interstitials can be present in dumbbell configurations [20]. The compensation of deficient charge has a different nature in this case and it is shown to be energetically more favorable in $In_2O_3$, as it is the predominant defect in the oxygen rich regime and Fermi energies within the band gap.

The charge deficiency is exclusively distributed over two atoms giving rise to a rather localized charge distribution by the formation of a covalent bond, whereas other atoms in the structure remain largely unaffected. There is a slight imbalance in the amount of charge which is enclosed within the Bader volumes of the participating atoms, which can be attributed to the non-symmetric position of the dumbbell within the structure. The 'missing' deficient charge is located on an oxygen in the second neighbor shell of the dumbbell. The excess charge on the dumbbell can be approximated by the sum of the total charge within the Bader volumes of the dimer atoms minus the amount of electrons nominally brought in by an oxygen atom within the calculation. This yields a net Bader charge of 7.3 electrons for the dimer compared with 7.2 electrons of a lattice oxygen in the ideal structure, indicating a doubly negative charged peroxo-ion configuration ($O_2^{2-}$) similar to the configuration described in [20] for ZnO. The reaction of the dimer on removal of electrons is a shorter bond length in order to compensate for the loss of electron density. The bond length changes from 1.37 Å for the charge state $q = +2$ to 1.51 Å for $q = -1$. Additionally, the dimer tends to move towards a third oxygen atom showing a slight lack of charge. Except for the dimer atoms the lattice relaxations are rather small. Therefore, there are various ways to accommodate an oxygen dumbbell within the host lattice.

The orientations of dumbbell defects with respect to the threefold symmetry axis are shown in figure 5 on the right and corresponding formation energies are shown in the middle part for the oxygen rich limit. There are two low energy configurations $O_{i,db}$ and $O_{i,db1}$, and another three having lower formation energies than regular *c*-site interstitials. The orientation of the most stable dumbbell ($O_{i,db}$) lies within a {100} plane and is aligned (as much as possible) with two neighboring interstitial *c*-sites along the ⟨110⟩ directions (figure 6). The high electron concentration between the participating atoms indicates covalent bonding. In the electronic band structure two highly localized defect states for the dumbbell configuration (figure 4) can be identified, whereas *c*-site interstitials exhibit three atomic orbital like oxygen acceptor defect bands with a strong p-character. In the first case the discrete energy levels of a peroxo molecule can be identified, whereas in the latter case the states resemble the three atomic states of an isolated oxygen ion.

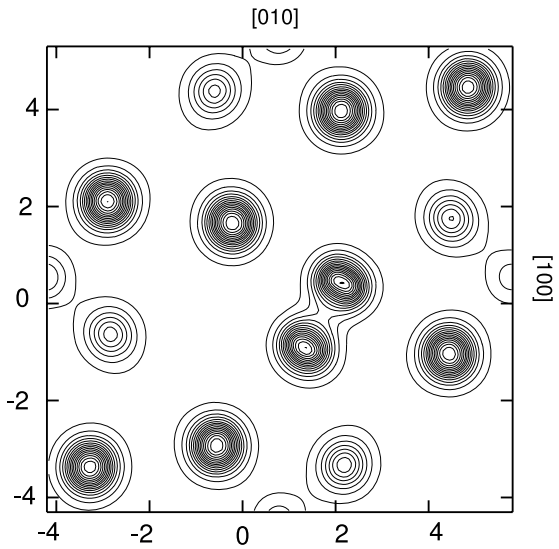


**Figure 6.** Charge density plot showing the arrangement of the oxygen dumbbell interstitial ($O_{i,db}$) within an oxygen (100) plane. The oxygen atoms have differing densities due to a varying elevation along [001]. The covalently bonded dumbbell is aligned between two symmetric interstitial *c*-sites denoted by vacant areas.

Furthermore, due to lack of symmetry, the defect states are not degenerate. The uppermost occupied defect bands can be identified as the anti-bonding $\pi^*_{p-p}$ molecular orbitals. The remaining oxygen dimer molecular orbitals are also highlighted in the figure. For this defect, adding electrons would result in the occupancy of the conduction band since the $\sigma^*_{p-p}$ states can be found only 2.2 eV above the CBM. Therefore no ambipolar behavior can be established for this defect type. The charge state $q = -1$ denotes only a very shallow energy minimum on the total energy surface for the oxygen dumbbells giving a transition level $\epsilon(0/-1)$ far beyond the CBM. The remarkable stability of this defect is caused by the binding $\sigma_{p-p}$ states which are located about one 1 eV below the valence band minimum.

*3.2.4. Stability of oxygen interstitial configurations.* We also investigated the kinetic barriers separating different interstitial configurations. In order to determine the transition energy, we used the nudged elastic band-climbing image (NEB-CI) method [37–39]. Barrier energies were found to be below 0.3 eV for barriers between the different covalent structures. For neutral charge states the symmetric interstitial defect configurations have barriers significantly lower than 0.1 eV for transitions into oxygen dumbbells. Obviously, these positions will undergo instantaneous transition into dumbbells at finite temperatures. Surprisingly, the highly symmetric interstitial *a*-site is not a stable interstitial configuration for oxygen in any charge state, whereas it is stable for indium interstitials (0.9 eV barrier energy). In summary the $O_{i-c}$ defect is the only stable interstitial defect configuration at high Fermi energy ($q = -2/-1$), whereas the dumbbells are the stable defect structures at lower Fermi energy, and transformations into other covalent structures can occur. In particular, the different

dumbbell geometries denote low energy transition paths for atomic movement.

*3.2.5. Indium vacancies.* Compared with oxygen interstitials, the indium vacancies play a minor role as an acceptor or electron killer defect. Except for very high Fermi energies, the formation energies are higher than for oxygen interstitials. For highly doped $In_2O_3$ (ITO) a transition could occur from a donor compensation by oxygen interstitials to indium vacancies. This is possible since the favored charge states for indium vacancies ($q = -3$) and oxygen interstitials ($q = -2$) are different at high Fermi energy. The indium vacancy possesses transition levels to lower charge states throughout the band gap, but the formation energies attain high values for these Fermi levels. Energetically, the difference between vacancies on the two distinct indium sites ($V_{In-b}$ and $V_{In-b}$) is less than 0.1 eV for all charge states. For both configurations a strong outward relaxation (13%) of the six neighboring oxygen can be found with a strong localization of surplus charge on the neighboring oxygen atoms. The relaxation is independent of the charge state and only found within the first neighbor shell. Different compensating defect types have been already discussed in the literature [7, 46–48], for tin-doped material but the differences have been attributed to interstitials in different defect complexes with tin. As the tin concentrations may become extremely high [7] ($10^{22}$ cm$^{-3}$) further defect interactions have to be accounted for in order to elucidate the relevance of indium vacancies for charge compensation. However, as indium defects are likely to have lower mobility than oxygen atoms, indium vacancies could be a candidate for non-reducible compensating defects [7, 48].

### *3.3. Finite-size and band gap corrections*

Since the finite-size effects as well as the known band gap error are of great importance we estimate the different error contributions in this section. Taking into account numerical aspects including all parameters the error of the total energies of the supercells can safely be estimated to be better than 0.01 eV. This accuracy is absolutely sufficient since for defect formation energies differences of rather different supercells are used and only a partial error cancelation can be expected. The introduced error is difficult to estimate but usually in the range of 0.1 eV [49]. Using only the Makov and Payne type correction a potentially large error may be introduced. Especially the static dielectric constant $\epsilon_r$ can change the formation energies significantly (∼1–2 eV). In this study the dielectric constant was taken from experiment. We have tested several different values for $\epsilon_r$ and found that the variation of the extrapolated value is not influenced as strong as the individual formation energies and the slopes by this choice. Using a wrong dielectric constant can even change the sign of the slope but still give a reasonable extrapolation value. Generally, we obtain better linear fits as a function of inverse volume if we apply the monopole correction instead of leaving them out. The typical extrapolation behavior is presented in figure 7 for the oxygen vacancy in all charge states. The scatter at higher charge states is probably caused by the different cell geometries which had to be used because of the large unit cell size (40 atoms). We have noticed that the potential alignment does never introduce an error larger than the extrapolation procedure for any charge state. The transition levels which are found within the conduction band (indium interstitials) are caused by an artificial band-filling effect which we have not corrected. This effect however only indicates the shallowness of the defect and does not change the results within the band gap region. Finally, and in order to obtain defect concentrations it is necessary to correct for the band gap error. Most commonly a rigid shift of defect levels is assumed. However, in this case one had to increase the one particle energies of occupied defect levels. Often the correction is only applied on conduction states and the formation energy of donors increased by an energy equal of the difference in one particle energies times the occupation of the corresponding defect levels. The choice to only correct the conduction band, however, is usually not justified, and furthermore the change in energy does not include defect level relaxation and the double counting correction term using this scheme. Further, even with the GGA + $U$ the difference between calculated and experimental band gaps is at least 1 eV. The potential error which may be introduced by the application of a band gap correction of this simple kind is up to 3 eV (in the case of the neutral indium interstitial) and is therefore omitted in this study. Further, assuming that the GGA + $U$ indicates approximately the appropriate defect level shifts, one can observe the typical upward (but not rigid) shift for donors. On the other hand, acceptor levels shift downwards, which is not assumed by the simplified approach described earlier.

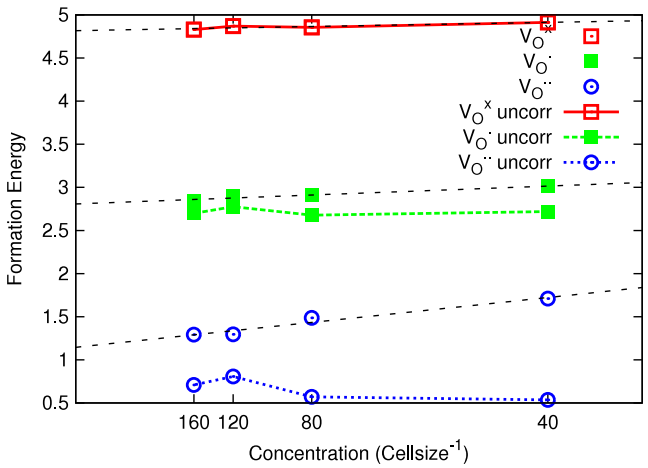


**Figure 7.** Extrapolation of the formation energies for the oxygen vacancy in its three different charge states. There is an increasingly strong cell size dependence for higher charge states. The fitting error increases for higher charge states. The scatter in the data is likely to be caused by different cell geometries used for calculations.

## 4. Summary and conclusion

By means of first-principle calculations within the plane wave pseudopotential formalism of density functional theory we have conducted an extensive study of various possible intrinsic point defect configurations in $In_2O_3$.

In case of donor defects the oxygen vacancy as well as the indium interstitial are in principle both capable of producing electrons within the conduction band, because positive charge states are favorable for Fermi energies over the whole band gap. Our calculations reveal that the oxygen vacancy is more likely to produce n-type behavior than the indium interstitials, due to its lower formation energy. Therefore the oxygen vacancy should be the major donor in $In_2O_3$ explaining the n-type conductivity as well as the non-stoichiometry. Moreover, we identify the distorted configuration of an indium antisite as a stable donor defect complex, and the association of donor defects to be energetically favorable for Fermi energies at the conduction band minimum.

For oxidizing conditions, there is a wealth of oxygen dumbbell-like defects which are thermodynamically stable. At low Fermi energies and oxygen rich conditions oxygen interstitials in dumbbell-like geometries, equivalent to doubly negative peroxo-ions, are identified as the dominant defect type. These oxygen dumbbells can efficiently compensate deficient charge because of their covalent oxygen bond. At higher Fermi energies, a transition from dumbbell-like configurations to doubly negative oxygen interstitials on symmetric *c*-sites occurs. Especially, for tin-doped samples, this symmetric oxygen interstitial is of importance since it compensates the positively charged donors at high dopant concentrations. It should be noted, however, that the indium vacancy occurs with an even higher charge state and comparable formation energy and therefore could also act as compensating defect at very high electron concentrations.

## Acknowledgment

We acknowledge the financial support through the Sonderforschungsbereich 595 'Fatigue of functional materials' of the Deutsche Forschungsgemeinschaft. Moreover, this work was made possible by grants for computing time on HHLR supercomputers at HRZ (TU-Darmstadt) and JSC at FZ-Jülich.

## References

[1] Hamberg I and Granqvist C G 1986 Evaporated Sn-doped $In_2O_3$ films: basic optical properties and applications to energy-efficient windows *J. Appl. Phys.* **60** R123

[2] Hartnagel H L, Dawar A K J and Jagadish C 1995 *Semiconducting Transparent Thin Films* (Bristol: Institute of Physics Publishing)

[3] Hung L S and Chen C H 2002 Recent progress in molecular organic electroluminescent materials and devices *Mater. Sci. Eng.* R **39** 143–222

[4] Brabec C J, Sariciftci N S and Hummelen J C 2001 Plastic Solar Cells *Adv. Funct. Mater.* **11** 15–26

[5] Peumans P, Yakimov A and Forrest S R 2003 Small molecular weight organic thin-film photodetectors and solar cells *J. Appl. Phys.* **93** 3693–723

[6] Ginley D S and Bright C 2000 Special issue on transparent conducting oxides *MRS Bull.* **25** 15–8

[7] Frank G and Köstlin G 1982 Electrical properties and defect model of tin-doped indium oxide layers *Appl. Phys.* A **27** 197–206

[8] Golovanov V *et al* 2005 Experimental and theoretical studies of indium oxide gas sensors fabricated by spray pyrolysis *Sensors Actuators* B **106** 563–71

[9] de Wit J H W 1977 Electron concentration and mobility in $In_2O_3$ *J. Solid State Chem.* **38** 819

[10] de Wit J H W 1975 The high temperature behavior of $In_2O_3$ *J. Solid State Chem.* **13** 192–200

[11] Scott J C, Kaufman J H, Brock P J, DiPietro R, Salem J and Goitia J A 1996 Degradation and failure of MEH-PPV light-emitting diodes *J. Appl. Phys.* **79** 2745–51

[12] Tanaka I, Tatsumi M, Nkano M and Adachi H 2002 First-principles calculations of anion vacancies in oxides and nitrides *J. Am. Ceram. Soc.* **85** 68–74

[13] Tanaka I, Oba F, Tatsumi K, Kunisu M, Nkano M and Adachi H 2002 First-principles calculations of anion vacancies in oxides and nitrides *Mater. Trans.* **7** 1426–9

[14] Tomita T, Yamashita K, Hayafuji Y and Adachi H 2005 The origin of n-type conductivity in undoped $In_2O_3$ *Appl. Phys. Lett.* **87** 051911

[15] Lany S and Zunger A 2007 Dopability, intrinsic conductivity, and nonstoichiometry of transparent conducting oxides *Phys. Rev. Lett.* **98** 045501

[16] Walsh A *et al* 2008 Nature of the band gap of $In_2O_3$ revealed by first-principles calculations and x-ray spectroscopy *Phys. Rev. Lett.* **100** 167402

[17] Weiher R L and Ley R P 1966 Optical properties of indium oxide *J. Appl. Phys.* **37** 299

[18] Klein A 2000 Electronic properties of $In_2O_3$ surfaces *Appl. Phys. Lett.* **77** 2009

[19] Fuchs F and Bechstedt F 2008 Indium-oxide polymorphs from first principles: quasiparticle electronic states *Phys. Rev.* B **77** 155107

[20] Erhart P, Klein A and Albe K 2005 First-principles study of the structure and stability of oxygen defects in zinc oxide *Phys. Rev.* B **72** 085213

[21] Kresse G and Furthmüller J 1996 Efficient iterative schemes for *ab initio* total-energy calculations using a plane-wave basis set *Phys. Rev.* B **54** 11169

[22] Kresse G and Furthmüller J 1996 Efficiency of *ab initio* total energy calculations for metals and semiconductors using a plane-wave basis set *Comput. Mater. Sci.* **6** 15–50

[23] Blöchl P E 1994 Projector augmented-wave method *Phys. Rev.* B **50** 17953–79

[24] Kresse G and Joubert D 1999 From ultrasoft pseudopotentials to the projector augmented-wave method *Phys. Rev.* B **59** 1758–75

[25] Perdew J P, Burke K and Ernzerhof M 1996 Generalized gradient approximation made simple *Phys. Rev. Lett.* **77** 3865–8
Perdew J P, Burke K and Ernzerhof M 1997 *Phys. Rev. Lett.* **78** 1396 (erratum)

[26] Dudarev S L, Botton G A, Savrasov S Y, Humphreys C J and Sutton A P 1998 Electron-energy-loss spectra and the structural stability of nickel oxide: an LSDA + $U$ study *Phys. Rev.* B **57** 1505–9

[27] Erhart P, Klein A, Egdell R G and Albe K 2007 Band structure of indium oxide: indirect versus direct band gap *Phys. Rev.* B **75** 153205

[28] Anisimov V I, Zaanen J and Andersen O K 1991 Band theory and Mott insulators: Hubbard $U$ instead of stoner I *Phys. Rev.* B **44** 943–54

[29] Liechtenstein A I, Anisimov V I and Zaanen J 1995 Density-functional theory and strong interactions: orbital ordering in Mott–Hubbard insulators *Phys. Rev.* B **52** R5467–70

[30] Barr T L and Liu Y L 1989 An x-ray photoelectron spectroscopy study of the valence band structure of indium oxides *J. Phys. Chem. Solids* **50** 657

[31] Piper L F J *et al* 2009 Electronic structure of $In_2O_3$ from resonant x-ray emission spectroscopy *Appl. Phys. Lett.* **94** 022105

[32] Erhart P, Albe K and Klein A 2006 First-principles study of intrinsic point defects in ZnO: role of band structure, volume relaxation and finite size effects *Phys. Rev.* B **73** 205203

[33] Makov G and Payne M C 1995 Periodic boundary conditions in *ab initio* calculations *Phys. Rev.* B **51** 4014–22

[34] Lento J, Mozos J L and Nieminen R M 2002 Charged point defects in semiconductors and the supercell approximation *J. Phys.: Condens. Matter* **14** 2637–45
[35] Persson C, Zhao Y J, Lany S and Zunger A 2005 n-type doping of $CuInSe_2$ and $CuGaSe_2$ *Phys. Rev.* B **72** 035211
[36] Bader R F W 1990 *Atoms in Molecules—A Quantum Theory* (Oxford: Oxford University Press)
[37] Henkelman G, Jóhannesson G and Jónsson H 2000 Methods for finding saddlepoints and minimum energy paths *Progress on Theoretical Chemistry and Physics* ed S D Schwartz (Dordrecht: Kluwer Academic) p 269
[38] Henkelman G and Jónsson H 2000 Improved tangent estimate in the nudged elastic band method for finding minimum energy paths and saddle points *J. Chem. Phys.* **113** 9978–85
[39] Henkelman G, Uberuaga BP and Jónsson H 2000 A climbing image nudged elastic band method for finding saddle points and minimum energy paths *J. Chem. Phys.* **113** 9901–4
[40] Zhang S B and Northrup J E 1991 Chemical potential dependence of defect formation energies in GaAs: application to Ga self-diffusion *Phys. Rev. Lett.* **67** 2339–42
[41] Qian GX, Martin RM and Chadi DJ 1988 First-principles study of the atomic reconstructions and energies of Ga- and As-stabilized GaAs(100) surfaces *Phys. Rev.* B **38** 7649
[42] Gassenbauer Y *et al* 2006 Surface states, surface potentials and segregation at surfaces of tin-doped $In_2O_3$ *Phys. Rev.* B **73** 245312
[43] Lany S and Zunger A 2005 Anion vacancies as a source of persistent photoconductivity in II–VI and chalcopyrite semiconductors *Phys. Rev.* B **72** 035215
[44] Mryasov O N and Freeman A J 2001 Electronic band structure of indium tin oxide and criteria for transparent conducting behaviour *Phys. Rev.* B **64** 233111
[45] Kilic C and Zunger A 2002 Origins of coexistence of conductivity and transparency in $SnO_2$ *Phys. Rev. Lett.* **88** 095501
[46] Warschkow O, Ellis D E, González G B and Mason T O 2003 Defect structure of tin-doped indium oxide *J. Am. Ceram. Soc.* **86** 1700–6
[47] Warschkow O, Ellis D E, González G B and Mason T O 2003 Defect cluster aggregation and nonreducibility in tin-doped indium oxide *J. Am. Ceram. Soc.* **86** 1707–11
[48] Warschkow O, Miljacic L, Ellis D E, González G B and Mason T O 2006 Interstitial oxygen in tin-doped indium oxide transparent conductors *J. Am. Ceram. Soc.* **89** 616
[49] Van de Walle C G and Neugebauer J 2004 First-principles calculations for defects and impurities: applications to III-nitrides *J. Appl. Phys.* **95** 3851–79
[50] Marezio M 1966 Refinement of the crystal structure of indium oxide at two wavelength *Acta Crystallogr.* **20** 723–8
[51] Lide D R 2005 *Handbook of Chemistry and Physics* (Boca Raton, FL: CRC Press)